Vibration Control of Rotational Shell Structures Using Neural Network

Kiyotoshi Hiratsuka*
Kiyoshi Shingu**

*Department of Computer Science, Graduate School of Science and Technology,
Nihon University
7-24-1, Narashinodai, Funabashi-shi, Chiba 274-8501, JAPAN
TEL & FAX +81-474-69-5426
E-mail : kiyo@shinguu2.cs.cst.nihon-u.ac.jp

**Department of Oceanic Architecture and Engineering,
College of Science and Technology, Nihon University,
7-24-1, Narashinodai, Funabashi-shi, Chiba 274-8501, JAPAN
TEL&FAX +81-474-69-5426
E-mail : kshingu@shinguu2.cs.cst.nihon-u.ac.jp

Abstract

It has been proposed that neural network algorithm is applied to vibration control of a shell structure. The control object is a conical shell structure comprised of dampers which work in the vertical direction at the antinode of the first mode, and the damping ratio alternates between from 0.02 to 0.2. The purpose of control is the reduction of relative displacement to the ground at whole shell through adjusting damping ratio. Controlling the shell, the Elman type neural network is employed and network weights are updated by on-line back-propagation procedure. Miyagiken-oki earthquake is employed to input acceleration that is enlarged 2m/s^2. The control effects are estimated by comparison with non-control results.

1. Introduction

A wide variety of research on motion control using a neural network algorithm has widely been made. For example, the control algorithm was proposed by means of control simulation[1]. The algorithm of the motion control was estimated by means of artificial neural networks based on comparison of the analysis of the results of the physiological experiment with the biological neural networks[2]. Both of these research groups pay special attention to the flow of the learning method and information.

As the study for applications to the engineering of the motion/vibration control by means of the neural networks, for example, the autonomous underwater vehicles[3] and vibration control of cantilevers[4], the vibration control of a particles system structure[5], and other such work can be referred to.

Shallow rotational shell structures are subjected to greater influence in the case of vertical motion than in the case of horizontal earthquakes[6]. Accordingly it is very important to lower the stress by restricting the vibration of the shells subjected to the vertical seismic forces[7].

Applications of the fuzzy vibration control of shell structures have been proposed by Shingu and Fukushima[7),8),9)]. Applications of the neural-network-based vibration control of a rigid-connection frame structure have been made at first by Hiratsuka and Shingu[5]. In the previous paper[10], an application of the vibration control using hierarchical neural networks was proposed in connection with the case where the vertical seismic forces act on a conical shell, and the vibration

control simulation is conducted.

In this paper, the Elman type neural network is used. Control results are estimated with non-control results (damping ratio:0.02 ; damping ratio:0.1115 which is the average damping ratio of the controlled one). The simulation results show that the displacements and the stresses in the shell with control are smaller than those in the shell without control. Then the conclusions show that the capability of neural-network-based vibration control of a shell is made clear and the control is very effective. In near future, we are going to apply the proposed control system to a real shell structure.

2. Vibration control of structure

Outline of a control method using a neural network for the shell structure is described in the following.

2.1 Flow of vibration control of shell

With vibration control of the shell, the control target, a settled value in connection with relative displacement complying with the ground, is zero. The displacement hereby referred to is the vertical displacement on a nodal point of the discrete shell structure. It is equivalent to the relative vertical displacement complying with the ground obtained by the measurement unit attached to the said nodal point in the case of the real structures. The control target is the settled value of zero, which stems from the reason why the stress becomes smaller as the relative displacement is made smaller to avoid collapse of the structure. Let it be understood that the input values to the controller are the vertical displacements of the time delay, the output data of the hidden layer in the neural network and acceleration of seismic wave. The control signals, which are fed to a damper attached to the shell structure, help change the viscosity of the damper and the vibration control of the shell is accomplished. The controller is the Elman type neural network, and the learning regulations will be in accordance with the back-propagation using the relative displacement as a consequence of the control. The flow of vibration control is shown in Fig.1.

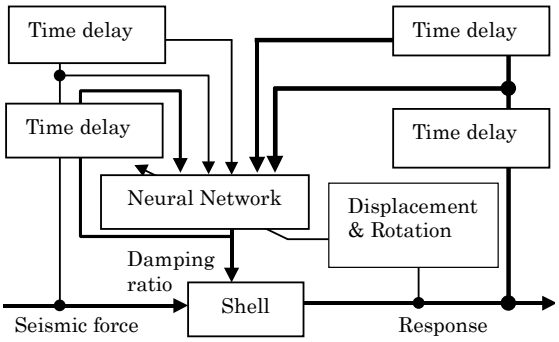

Fig. 1 Flow of vibration control

2.2 Fundamental equations of conical shell

The finite element method with conical frustum elements is used to analyze the shell. Usually, seismic waves have vertical and horizontal components. Vertical components are important for shallow shells subjected to seismic forces. Therefore the shell is treated as an axisymmetric problem[9].

2.2.1 Displacement functions

Displacements of an element in the meridional and normal direction u , w and the angle of rotation χ are represented in Eq. (1) by polynomials in the meridional distance S . $\alpha_1, \cdots, \alpha_6$ are unknown coefficients, and these are determined by the terminal conditions. The global and local coordinates of the conical frustum element are shown in Fig. 2.

$$\left.\begin{aligned} u &= \alpha_1 + \alpha_2 S \\ w &= \alpha_3 + \alpha_4 S + \alpha_5 S^2 + \alpha_6 S^3 \\ \chi &= dw/dS = \alpha_4 + 2\alpha_5 S + 3\alpha_6 S^2 \end{aligned}\right\} \quad (1)$$

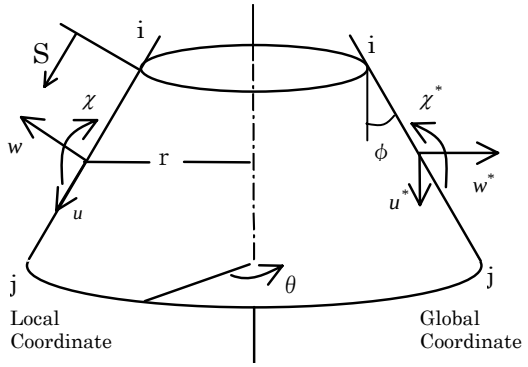

Fig. 2 Displacement components

2.2.2 Strain - displacement relation

Strains in the meridional and circumferential directions ε_S, ε_θ and changes in curvature κ_S, κ_θ are given in Eq. (2).

$$\begin{Bmatrix} \varepsilon_S \\ \varepsilon_\theta \\ \cdots \\ \kappa_S \\ \kappa_\theta \end{Bmatrix} = \begin{Bmatrix} du/dS \\ (u\sin\phi + w\cos\phi)/r \\ \cdots\cdots\cdots\cdots \\ -d^2w/dS^2 \\ -(\sin\phi/r)\cdot dw/dS \end{Bmatrix} \quad (2)$$

2.2.3 Stress – Strain relation

Stress resultants in the meridional and circumferential directions N_S, N_θ and bending moments M_S, M_θ are given in Eq. (3). Components of stress resultans are shown in Fig.3.

$$\begin{Bmatrix} N_S \\ N_\theta \\ \cdots \\ M_S \\ M_\theta \end{Bmatrix} = \begin{Bmatrix} k & \nu k & \vdots & 0 & \\ \nu k & k & \vdots & & \\ \cdots\cdots & & \vdots & \cdots\cdots & \\ 0 & & \vdots & D & \nu D \\ & & \vdots & \nu D & D \end{Bmatrix} \begin{Bmatrix} \varepsilon_S \\ \varepsilon_\theta \\ \cdots \\ \kappa_S \\ \kappa_\theta \end{Bmatrix} \quad (3)$$

where

$k = Et/(1-\nu^2), D = Et^3/12(1-\nu^2)$

E =Young's modulus, ν =Poisson's ratio, and t =shell thickness

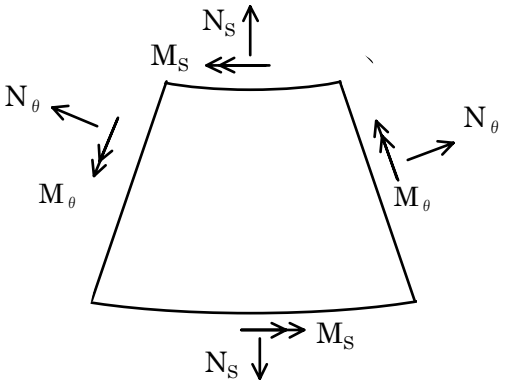

Fig. 3 Stress resultants

2.3 Control Object

The control object is the conical shell structure that is comprised of dampers, which work in the vertical direction at the antinode of the first mode. The section of the controlled shell is shown in Fig. 4 and the configuration of a damper is shown in Fig. 5. And the step-by-step integration method is used for the vibration analysis of the conical shell[8]. This method is considered on the variable damping ratio. Then the lumped mass matrix is used. The vibration equation is expressed in Eq. (4). The geometrical and material constants of the shell are shown in Table 1.

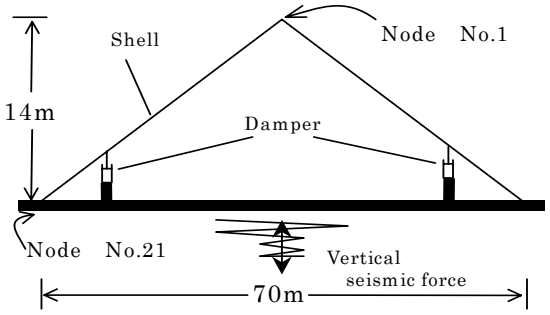

Fig. 4 Conical shell with dampers

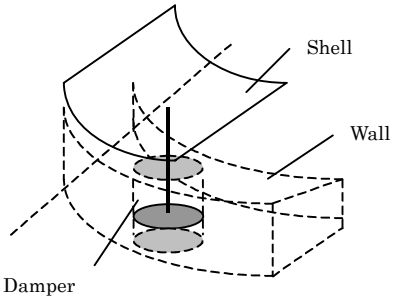

Fig. 5 Configuration of damper

Table 1 Geometrical and material constants of shell

rise	$H = 14\,m$
span	$l = 70\,m$
shell thickness	$t = 1.0\ m$
Young's modulus	$E = 1.3524 \times 10^{-3}\ \mathrm{N/m^2}$
Poisson's ratio	$\nu = 0$
mass Density	$\rho = 400\ \mathrm{kg/m^3}$

$$[M]\{\ddot{d}\} + [C]\{\dot{d}\} + [K]\{d\} = -f\{m\} \quad (4)$$

where

$[M]$, $[K]$: mass and stiffness matrix of shell

$\{\ddot{d}\} = \{\ddot{u}_1^*, \ddot{w}_1^*, \ddot{\chi}_1^*, \cdots, \ddot{u}_{20}^*, \ddot{w}_{20}^*, \ddot{\chi}_{20}^*\}$

: acceleration vector

$\{\dot{d}\} = \{\dot{u}_1^*, \dot{w}_1^*, \dot{\chi}_1^*, \cdots, \dot{u}_{20}^*, \dot{w}_{20}^*, \dot{\chi}_{20}^*\}$

: velocity vector

$\{d\} = \{u_1^*, w_1^*, \chi_1^*, \cdots, u_{20}^*, w_{20}^*, \chi_{20}^*\}$

: displacement vector

$u_i^*, w_i^*, \chi_i^* \ (i = 1, \cdots, 20)$

: vertical, horizontal displacements and angle of rotation, respectively

f : acceleration of seismic force

$\{m\} = \{m_1, 0, 0, m_2, 0, 0, \cdots, m_{20}, 0, 0\}^T$

: mass vector

$1, \cdots, 20$: node number without supported end

The total element and node numbers are 20 and 21, respectively. The node numbers are 1 at the top, and 21 at the supported end. The damper is attached at node 14. The boundary condition is the fixed end.

Damping matrix and damping ratios are as follows:

$$[C] = 2\omega_1 \text{diag.}(m_1\zeta_1, m_1\zeta_1, m_1\zeta_1, \cdots, m_{13}\zeta_{13}, m_{13}\zeta_{13}, m_{13}\zeta_{13}, m_{14}\zeta(t), m_{14}\zeta_{14}, m_{14}\zeta_{14}, m_{15}\zeta_{15}, m_{15}\zeta_{15}, m_{15}\zeta_{15}, \cdots, m_{20}\zeta_{20}, m_{20}\zeta_{20}, m_{20}\zeta_{20}) \quad (5)$$

$\zeta_i = 0.02 \ (i = 1, \cdots, 20)$

$0.02 \le \zeta(t) \le 0.2$: damping ratio at the antinode of the first mode

ω_1 : first natural circular frequency

2.4 Neural network

The controller utilized here is the 3-layer hierarchical neural network as mentioned above (see Fig.6). Each function at a unit in the hidden and the output layer is the sigmoid function.

The sigmoid function is as follows.

$$s(x) = \frac{1}{1+e^{-x}} \quad (6)$$

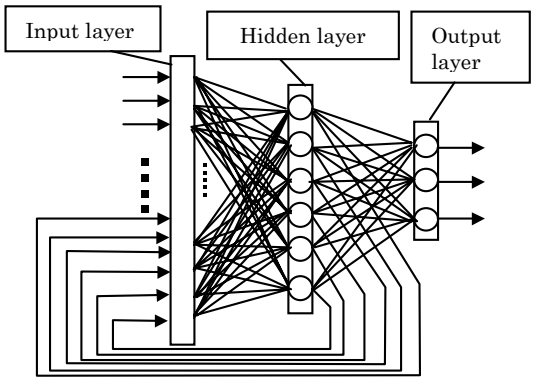

Fig. 6 Neural netwrok

2.5 Flow of control simulation

The control simulation is repeated in the following procedures from (i) to (iv). Dynamic analysis of the shell is carried out at 0.002 seconds interval, and the shell is controlled at 0.02 seconds interval.

(i) Input into the neural network

There are 362 units in the input layer, 181 units in the hidden layer and 1 unit in the output layer. The functions of the units in the hidden and the output layer are sigmoid functions described above. The input data to the network at time $t+\tau+h$ are the displacement, acceleration of seismic wave at time $t+\tau$ and $t+\tau-h$, the output data of the hidden layer in the neural network at time $t+\tau$. Here t, h and τ are time, a small time interval during the integration and a time interval of the control, respectively. The output data are calculated by Eqs. (7) and (8).

The value of the unit in the hidden layer y_i is as follows.

$$y_j = s\left(\sum_{k=1}^{63} w_{jk}^{(1)} x_k - \vartheta_j\right) \quad (7)$$

$(j = 1, \cdots, 21)$

where

$w_{jk}^{(1)}$: weight of connection between the hidden and the input layer

ϑ_j : thresholds of the units in the hidden layer

The value of the unit in the output layer is as follows.

$$o_i = s\left(\sum_{j=1}^{21} w_{ij}^{(2)} y_j - \varphi_i\right) \quad (i = 1,2,3) \tag{8}$$

where

$w_{ij}^{(2)}$: weight of connection between the output layer

φ_i : thresholds of the units in the output layer

The input data are shown in Eq.(9).

$$\{x_1, \cdots, x_{63}\} = \{u^*_{t+\tau-h,1}, \cdots, u^*_{t+\tau-h,20}, u^*_{t+\tau,1}, \cdots, u^*_{t+\tau,20}, y_{t+\tau,1}, \cdots, y_{t+\tau 21}, f_{t+\tau-h}, f_{t+\tau}\} \tag{9}$$

where

u^* : vertical displacement

$y_{t+\tau,i}$: output of the hidden layer in the neural network at time $t+\tau$ $(i = 1,...,21)$

index h : small time interval during integration $(= 0.002(\text{sec}))$

index τ : time interval of control $(= 0.02(\text{sec}))$

(ii) Calculation of damping ratio

The damping ratio is computed at time $t+\tau+h$ from the output of the neural network by Eq. (10).

$$\varsigma(t+\tau+h) = (o_1 - o_2 + 1)\cdot o_3 + 0.09 \cdot o_3 + 0.02 \tag{10}$$

where

if $\varsigma(t+\tau+h) \geq 0.2$ then $\varsigma(t+\tau+h) = 0.2$

(iii) Response analysis

The dynamic response of the shell is computed by the step-by-step integration method[8]. The equations are shown as follows.

$$\{d\}_{t+h} = [E]^{-1}\left([G]\{d\}_t + [V]\{v\}_t + [A]\{a\}_t + \beta h^2 \{F\}_{t+h}\right) \tag{11}$$

$$\{v\}_{t+h} = \left(\frac{h}{2}\{d\}_{t+h} - \frac{h}{2}\{d\}_t - \left(\frac{1}{2} - \beta\right)h^2\{v\}_t - \left(\frac{1}{4} - \beta\right)h^3\{a\}_t\right) \Big/ \left(\beta h^2\right) \tag{12}$$

$$\{a\}_{t+h} = \left(\{d\}_{t+h} - \{d\}_t - h\{v\}_t - \left(\frac{1}{2} - \beta\right)h^2\{a\}_t\right) \Big/ \left(\beta h^2\right) \tag{13}$$

where

$$[E] = [M] + \frac{h}{2}[C]_{t+h} + \beta h^2 [K] \tag{14}$$

$$[A] = \left(\frac{1}{2} - \beta\right)h^2[M] + \left(\frac{1}{4} - \beta\right)h^3[C]_{t+h} \tag{15}$$

$$[V] = h[M] + \left(\frac{1}{2} - \beta\right)h^2[C]_{t+h} \tag{16}$$

$$[G] = [M] + \frac{h}{2}[C]_{t+h} \tag{17}$$

β : acceleration coefficient $(= 1/4)$

h : small time interval $(= 0.002)$

(iv) Learning

During the control, the neural network makes learning sequentially. The learning regulation is a renovation method of the weight of the network. The learning means renovating the weight of the network using the input data and control results in accordance with the learning regulations. The learning regulations will renovate the weight in a method in accordance with back-propagation. The learning is made by changing the weight of the network using the displacement in the case of time $t+\tau+h$. Change of the weight is calculated in accordance with the equation shown below. The value of weights and thresholds are evaluated by Eqs. (18) - (22) and those are renovated by Eqs. (23) - (26). η is equal to 0.0021.

$$\delta E = \eta D \tag{18}$$

where

$$D = b_{i_0}$$

$$\{b\} \equiv \{ u^*_{t+\tau+h,1}, w^*_{t+\tau+h,1}, \chi^*_{t+\tau+h,1}, \cdots , u^*_{t+\tau+h,20}, w^*_{t+\tau+h,20}, \chi^*_{t+\tau+h,20} \}$$
$$\equiv \{ b_1, \cdots, b_{60} \}$$
$$|A| = \max_{1 \le i \le 60} |b_i|$$
$$i_0 = \max \{ i \mid |b_i| = |A|, i = 1, \cdots, 60 \}$$

$$\delta w^{(2)}_{ij} = \delta E \, o_i (1 - o_i) \, u_j \quad (19)$$
$$\delta \varphi_i = \delta E \, o_i (1 - o_i) \quad (20)$$
$$\delta w^{(1)}_{jk} = \sum_{i=1}^{3} \delta E \, o_i (1 - o_i) w^{(2)}_{ij} u_j (1 - u_j) x_k \quad (21)$$
$$\delta \vartheta_j = \sum_{i=1}^{3} \delta E o_i (1 - o_i) w^{(2)}_{ij} u_j (1 - u_j) \quad (22)$$
$$w^{(2)}_{ij} \leftarrow w^{(2)}_{ij} + \delta w^{(2)}_{ij} \quad (23)$$
$$\varphi_i \leftarrow \varphi_i + \delta \varphi_i \quad (24)$$
$$w^{(1)}_{jk} \leftarrow w^{(1)}_{jk} + \delta w^{(1)}_{jk} \quad (25)$$
$$\vartheta_j \leftarrow \vartheta_j + \delta \vartheta_j \quad (26)$$
$$(i = 1,2,3)$$
$$(j = 1, \cdots, 181)$$
$$(k = 1, \cdots, 362)$$

3. Natural vibration

3.1 Analytical method

EISPACK in 1988 is used to solve the eigen value problem. EISPACK is a collection of Fortran subroutines that compute the eigenvalues and eigenvectors of nine classes of matrices: complex general, complex Hermitian, real general, real symmetric, real symmetric banded, real symmetric tridiagonal, special real tridiagonal, generalized real, and generalized real symmetric matices. In addition, two routines are included that use singular value decomposition to solve certain least-squares problems[11].

3.2 Results

Natural frequencies are shown in Table 2 and the corresponding natural vibration modes in the vertical components are shown in Fig. 7.

Table 2 Natural frequency

Order	1st	2nd	3rd
Frequency(Hz)	4.78	6.96	10.02

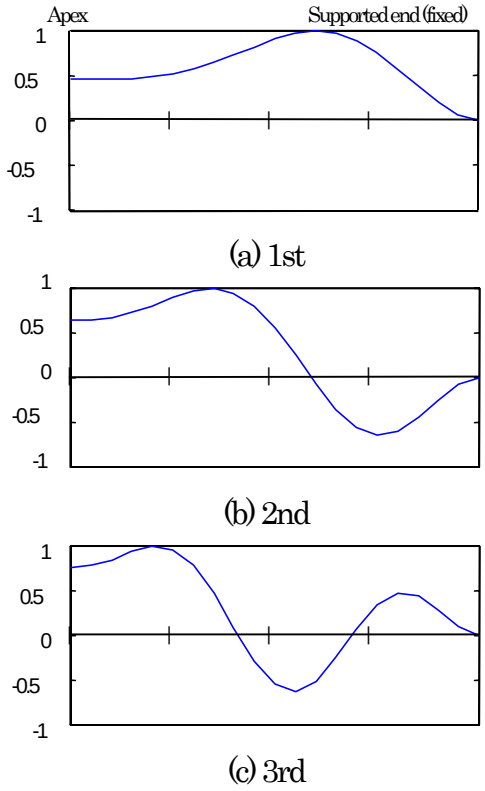

Fig. 7 Natural vibration modes

4. Simulation results

Fig.8 shows Miyagiken-oki earthquake used for input acceleration, where the maximum acceleration is enlarged to 2 m/sec^2. The control effects are estimated by comparison with non-control results. These results are shown in Figs.9 - 21. The meanings of symbols, NON, AVG and CONT are as follows:

NON: Non-control (damping ratio: 0.02)

AVG: Non-control (damping ratio: 0.1115, which is average damping ratio of controlled one)

CONT: Control

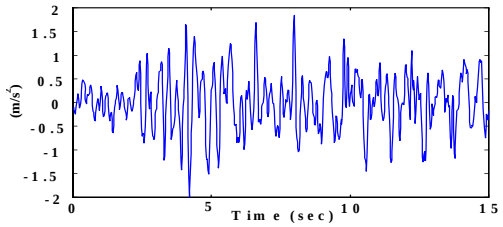

Fig.8 Miyagiken-oki earthquake, Japan, UD, June 12,1978

4.1 Maximum displacements

Figs. 9 and 10 show the maximum displacements in the vertical and horizontal directions, respectively.

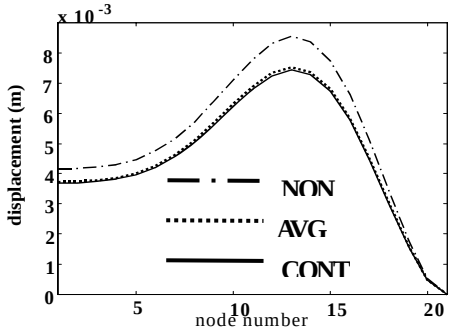

Fig. 9 Vertical displacements u^*

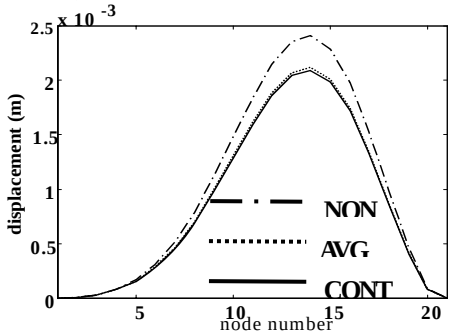

Fig. 10 Horizontal displacements w^*

4.2 Maximum stresses

Figs. 11 and 12 show the maximum axial forces N_S and N_θ, and Figs. 13 and 14 show the maximum bending moments M_S and M_θ, respectively. The node 13 has the maximum value in Figs 9 and 10. Table 3 shows values of N_S, N_θ, M_S and M_θ at the node 13.

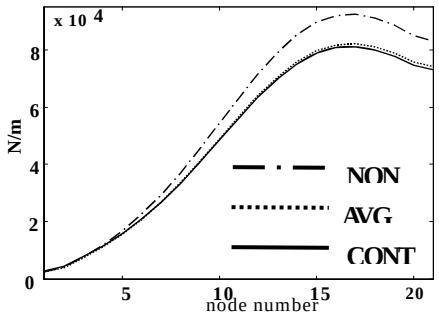

Fig. 11 Axial force N_S

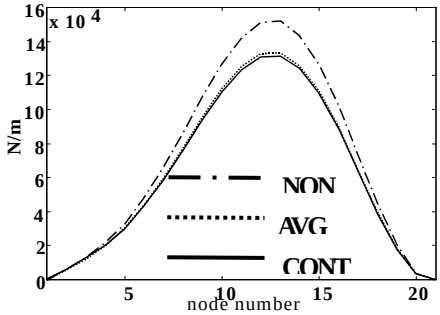

Fig. 12 Axial forces N_θ

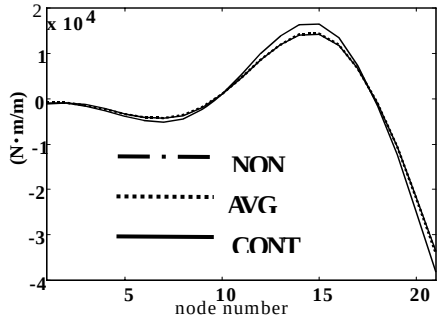

Fig. 13 Bending moments M_S

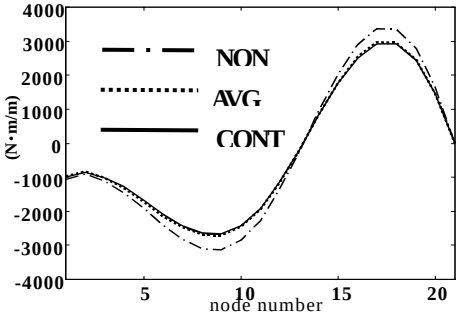

Fig. 14 Bending moments M_θ

Table 3 Comparison of stresses at node 13

	NON	AVG	CONT
N_S (N/m)	79160	70583	69819
N_θ (N/m)	143490	125780	12428
M_S (N·m/m)	16931	11984	11933
M_θ (N·m/m)	931.72	819.80	815.15

4.3 Time history and average of damping ratio

Time history of the damping ratio is shown in Fig.15.

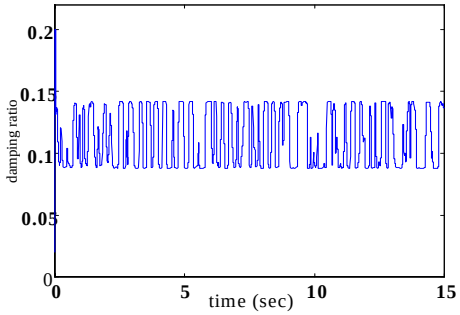

Fig. 15 Time history of damping ratio

Non-controlled damping ratio: 0.02
Average of controlled damping ratio: 0.1115

4.4 Time history of damping force

The damping force of the damper is computed by Eq. (26). Time histories of the damping ratios are shown in Figs.16 - 18.

$$F_d = 2\omega_1 \zeta m_{14} \dot{u}_{14}^* \qquad (26)$$

where

F_d : damping force of damper

ω_1 : the first natural circular frequency

$$\zeta = \begin{cases} 0.02 & : \text{NON} \\ \zeta(\tau) & : \text{CONT} \\ \bar{\zeta} & : \text{AVG} \end{cases}$$

m_{14} : mass at node 14

$\dot{u}_{14}^*$: velocity at node 14 in the vertical direction

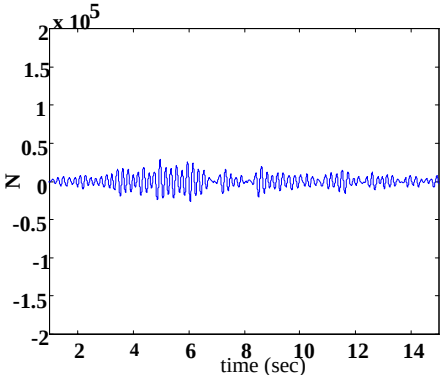

Fig. 16 Time history of damping force at node 14 (NON)

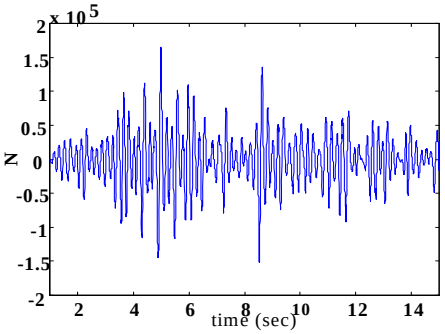

Fig. 17 Time history of damping force at node 14 (CONT)

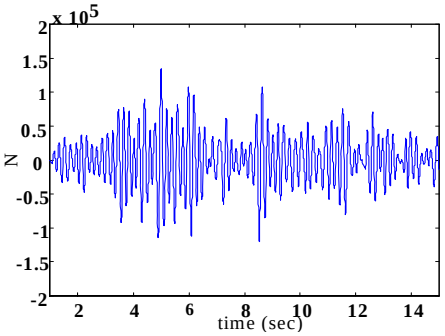

Fig. 18 Time history of damping force at node 14 (AVG)

4.5 Time history of work rate of damping force

The work rate of the damping force at node 14 is computed by Eq. (27). Time histories of work rates of damping force are shown in Figs. 19 - 21.

$$\Delta W = F_d \cdot \dot{u}_{14}^* \qquad (27)$$

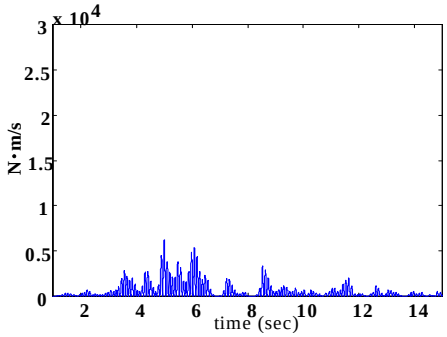

Fig.19 Time history of work rate of damping force at node 14 (NON)

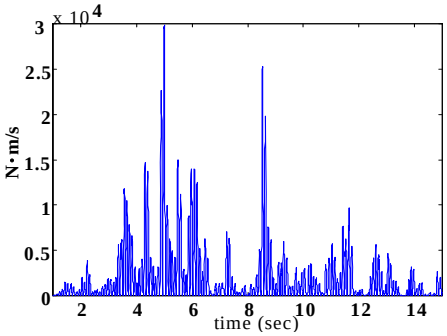

Fig.20 Time history of work rate of damping force at node 14 (CONT)

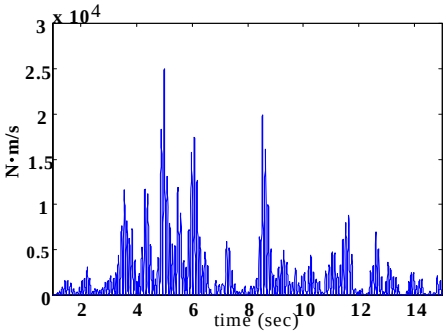

Fig.21 Time history of work rate of damping force at node 14 (AVG)

5. Observation

The following analytical results are obtained from the research.

1) With respect to the maximum response displacement in the vertical and horizontal directions, the controlled (CONT) results are reduced by 11% of the non-controlled (NON) ones, and by 2% of the AVG results.

2) With respect to the maximum stresses of N_s, N_θ, M_s and M_θ, the CONT results are reduced by 12% of the NON ones, and by 2% of the AVG ones.

4) With respect to the maximum damping force, the CONT result are 5.8 times of the NON ones, and 1.2 of the AVG ones.

5) With respect to the work rate of damping force, the CONT results are 4.7 times of the NON ones, and 1.2 of the AVG ones.

6) With respect to the time history of displacement u_{14}^* and the work rate of damping force ΔW relation, ΔW of the CONT results is greater than those of the NON and AVG ones when displacement u_{14}^* is small.

6. Conclusions

The displacements and stresses in the shell under the CONT are smaller than those of the NON and the AVG.

The vibration control in the shell with neural networks proposed in this paper restricts the displacements and stresses in the shell.

Acknowledgement

This study was supported in part the Nihon University College of Science and Technology Special Grant-in-Aid Recommended Research (Representative : K. Shingu).

Reference

1) Jordan, I. M. and Rumelhart, E. D.: Forward Models : Supervised Learning with a Distal Teacher, MIT Center for Cognitive Science, Occasional Paper #40

2) Kawato, M. and Gomi, H: Kinematics Model of The Human Brain, From Brain to Mind (Iwanami Shoten), pp235-244, 1995 (in Japanese)

3) Fujii, T. Ura, T. and Kuroda, Y.: Development of Self-Organizing Neural-Net-Controller System and Its Application to Underwater Vehicles, Journal of The Society of Naval Architects of Japan, Vol.168, pp.275-281 ,1990 (in Japanese)

4) Morishita, S. Kuroda, Y. and Ura, T.: Adaptive Vibration Control System with Controllable Dynamic Damper, Transaction of Japan Society of Mechanical Engineering, Vol.58, No.550 , pp1748-1754 , 1992 (in Japanese)

5) Hiratsuka, K. and Shingu, K.: A Study on Vibration Control of Multi-Degree-of-Freedom System Structure Using Neural Network Algorithm, Proceeding of the Conference on Computational Engineering and Science, Vol.2, No.2, pp677-680, 1997 (in Japanese)
6) Nishimura, T and Shingu, K: Study on Dynamic Response of Rotational Shells with Edge Beams Subjected to Seismic Forces in the Vertical and Horizontal Directions, Transaction of the Architectural Institute of Japan, Vol.326 , pp47－59, 1983 (in Japanese)
7) Shingu, K.: An Application of Fuzzy Theory to Vibration Control of a Shell Structure, Journal of Japan Society for Fuzzy Theory and Systems, Vol.9, No.2, pp162-169, 1997 (in Japanese)
8) Shingu, K and Fukushima, K: Study on Fuzzy Control of Shells Subjected to Seismic Forces Journal of Japan Society for Fuzzy Theory and Systems, Vol.5, No.3 , pp650-662 , 1993 (in Japanese)
9) Shingu, K. and Fukushima, K.: Seismic Isolation and Fuzzy Vibration Control of Shell Structure Subjected to Vertical Seismic Forces, Transaction of the Japan Society of Mechanical Engineers (C), Vol.60, No.577, pp2999-3005 , 1994 (in Japanese)
10)Hiratsuka,K and Shingu,K: Application of Neural Network to Vibration Control of Conical Shell Structures, THEORETICAL AND APPLIED MECHANICS, Vol. 47, 1998 (in press)
11)LAPACK – Linear Algebra PACKage, Users guide 2nd Edition